Quantifying the significance of coherence anomalies

Tengfei Lin[1], Thang Ha[1], Kurt J. Marfurt[1], and Kevin L. Deal[2]

Abstract

Semblance and other coherence measures are routinely used in seismic processing, such as velocity spectra analysis, in seismic interpretation to estimate volumetric dip and to delineate geologic boundaries, and in poststack and prestack data conditioning such as edge-preserving structure-oriented filtering. Although interpreters readily understand the significance of outliers for such measures as seismic amplitude being described by a Gaussian (or normal) distribution, and root-mean-square amplitude by a log-normal distribution, the measurement significance of a given coherence of poststack seismic data is much more difficult to grasp. We have followed early work on the significance of events seen in semblance-based velocity spectra, and we used an F-statistic to quantify the significance of coherence measures at each voxel. The accuracy and resolution of these measures depended on the bandwidth of the data, the signal-to-noise ratio (S/N), and the size of the spatial and temporal analysis windows used in their numerical estimation. In 3D interpretation, low coherence estimated not only the seismic noise but also the geologic signal, such as fault planes and channel edges. Therefore, we have estimated the S/N as the product of coherence and two alternative measures of randomness, the first being the disorder attribute and the second estimate based on eigenvalues of a window of coherence values. The disorder attribute is fast and easy to compute, whereas the eigenvalue calculation is computationally intensive and more accurate. We have demonstrated the value of this measure through application to two 3D surveys, in which we modulated coherence measures by our F-statistic measure to show where discontinuities were significant and where they corresponded to more chaotic features.

Introduction

Semblance and other coherence measures are routinely used in seismic processing, including for velocity spectra analysis (Taner and Koehler, 1969; Neidell and Taner, 1971), seismic edge detection and volumetric dip estimation (Marfurt et al., 1998), and edge-preserving structure-oriented filtering (Hoecker and Fehmers, 2002; Marfurt, 2006). The application of seismic attributes to depth-migrated data in which the wavelength extends by increasing the velocity with depth justifies the use of data-adaptive analysis windows, in which the window size is proportional to a percentile of the time or time- and space-varying spectra (Lin et al., 2014; T. Lin, personal communication, 2015).

In this paper, we reexamine the analysis by Douze and Laster (1979) on the significance of velocity-based semblance analysis to evaluate the significance of coherence anomalies within a noisy background, and the choice of parameters for structure-oriented filtering. These same concepts are readily generalized to eigenstructure-type coherence estimates.

We begin with a summary of semblance and KL-filter (energy ratio) coherence algorithms, as well as the use of the F-statistic. The F-statistic requires an estimate of the signal-to-noise ratio (S/N). We therefore evaluate Al-Dossary et al.'s (2014) disorder attribute and introduce a new S/N estimate based on the eigenvalues computed from a window of coherence. With these definitions in place, we apply our new metric to a coherence volume computed from a survey acquired in China. We conclude with a discussion on how such estimates may be useful in risk analysis, for differentiating different geologic features by their coherence expression, and for improved edge-preserving smoothing applications.

Theoretical analysis

Following Douze and Laster (1979) work, we generate a suite of figures to show the significance of typical windows used in edge detection and structure-oriented filtering. First, we define the significance of similarity (coherence) as the cumulative probability of a noncentral F-distribution. A high value of significance means the calculation of similarity is more reliable. In contrast, a low value of significance always indicates an unreliable similarity value. The range of the significance is 0–1 (see Appendix A).

[1]University of Oklahoma, ConocoPhillips School of Geology and Geophysics, Norman, Oklahoma, USA. E-mail: tengfei.lin@ou.edu; thang.n.ha-1@ou.edu; kmartfurt@ou.edu.

[2]Chevron Company, Houston, Texas, USA. E-mail: kevin.deal@chevron.com.

Manuscript received by the Editor 30 June 2015; revised manuscript received 10 October 2015; published online 18 April 2016; Pagination corrected 27 April 2016. This paper appears in *Interpretation*, Vol. 4, No. 2 (May 2016); p. T205–T213, 10 FIGS.

http://dx.doi.org/10.1190/INT-2015-0102.1.

Examining equation A-22, we identify four basic parameters in computing significance: bandwidth f_B, temporal analysis window size $2K\Delta t$, spatial analysis window size J, and the S/N. With these values, we can compute the significance of a given semblance estimate using the noncentral F-distribution. The product of the bandwidth and the vertical analysis window $2K\Delta t f_B$ determines the first degree of freedom, the number of seismic traces J determines the second degree of freedom, and S/N determines the noncentrality parameter.

Douze and Laster (1979) demonstrate that the correlation between band-limited experimental data and the theoretical cumulative probability distribution for broad-band data is quite good, allowing us to use this formalism for not only their velocity anomalies, but also our coherence attribute and structure-oriented filtering application. Meanwhile, considering the complexity of the significance algorithms, the calculation takes five times longer than the coherence code for typical parameters.

Applications

Example 1: A 2D synthetic of normally faulted layers

Figure 2a shows a simple model used to generate a suite of 200 finite-difference common-shot gathers. These gathers were then prestack time-migrated to generate the image shown in Figure 2b. There are five main layers B, C, and D, each of which contains five sublayers. To address the issue of S/N, we also added different levels of band-limited incoherent noise in layers B and C. The white arrow indicates a fault-plane reflection.

The images in Figure 3 form a matrix with vertical window sizes corresponding to 0, 10, and 20 ms along column, and lateral window sizes of 5, 9, and 13 analysis points along rows, by blending the similarity and the significance of coherence to illustrate the influence of spatial (number of seismic traces) and temporal analysis window size on the significance of similarity. With the increase of temporal analysis window size, the significance value of similarity is higher, which indicates that the coherence value is more reliable. The increase in the number of seismic traces shows a similar phenomenon, but the resolution of the fault zone decreases.

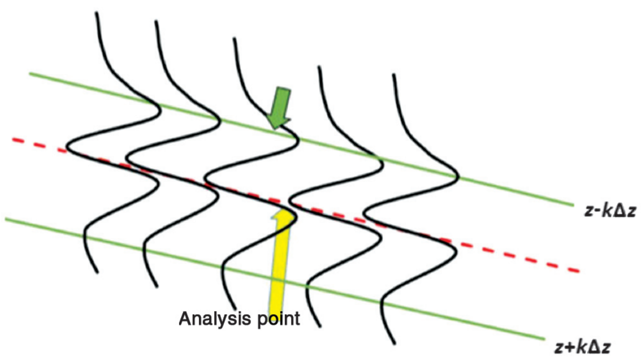

Figure 1. Two-dimensional diagram of similarity calculation.

Example 2: 3D seismic data over Bohai Bay Basin, China

We next compute the significance coherence computed from a 3D seismic volume acquired over Bohai Bay Basin, China that images a channel reservoir. Given the influence of d_1 (the vertical analysis window size) on significance, we introduce a self-adaptive window attribute calculation, defining the temporal window

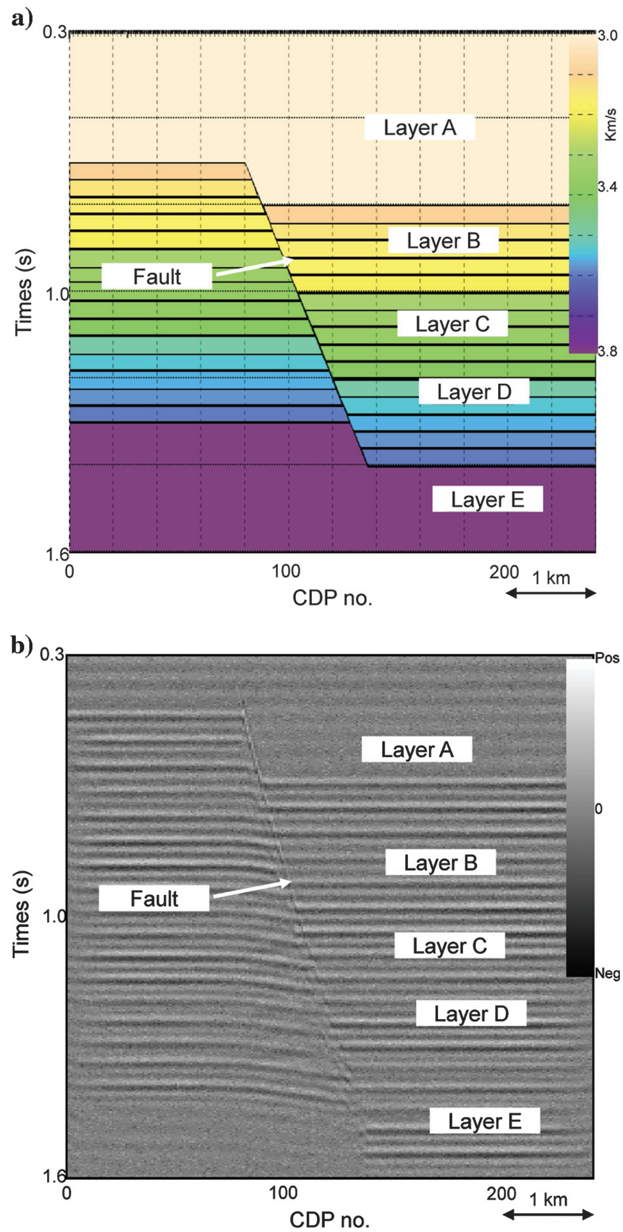

Figure 2. (a) The fault model and (b) the resulting image after forward modeling using a finite-difference algorithm and prestack Kirchhoff time migration. Band-limited random noise has been added resulting in $P_S/P_N = 1.0$.

to be propotional to the average frequency of each time slice. Figure 4 shows time slices at $t = 0.5$ s through seismic amplitde, peak frequency, and spectral bandwidth volumes using matching pursuit algorithm. The black arrow indicates a fault, the red arrow indicates a channel, and the blue arrow indicates an oxbow, which can be clearly seen in the coherence image shown in Figure 5.

Figure 5 shows slices at $t = 0.5$ s through coherence volumes computed using a self-adaptive temporal analysis window size, respectively. Black arrows indicate the main fault through the seismic slice. The inner bank of the oxbow lake can be indicated by the blue arrows, and three distinguished channels can be indicated by the red arrows.

Figure 6 shows the S/N corresponding to Figure 5 computed using equation A-11. The temporal analysis window size not only affects the degrees of freedom but also influences S/N, which indirectly controls the noncentrality parameter ε.

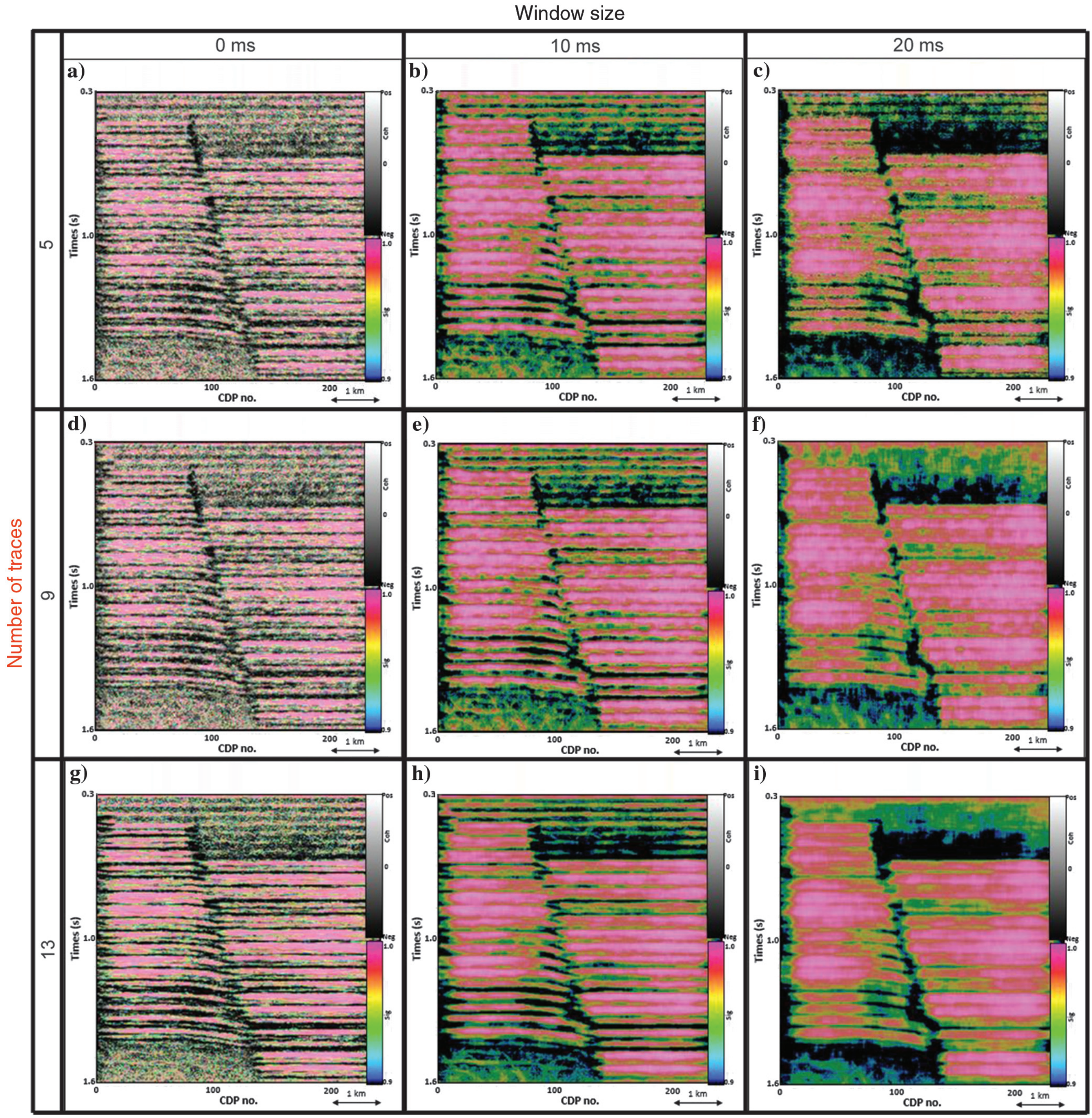

Figure 3. Vertical slice through similarity blended with significance of coherence computed from the seismic data shown in Figure 4 using a variable temporal analysis window size (0.0, 1.0, and 2.0 of mean period) and variable number of trace ($J = 5$, 9, and 13).

Figure 7 shows the sensitivity of significance to temporal analysis window size and bandwidth. The black arrows indicate the faults characterized by low coherence and significance. The red arrows indicate channel deposition or sheet sand characterized by high coherence and high significance. By computing the variable bandwidth and using a self-adaptive temporal analysis window size, we are able to improve the significance of

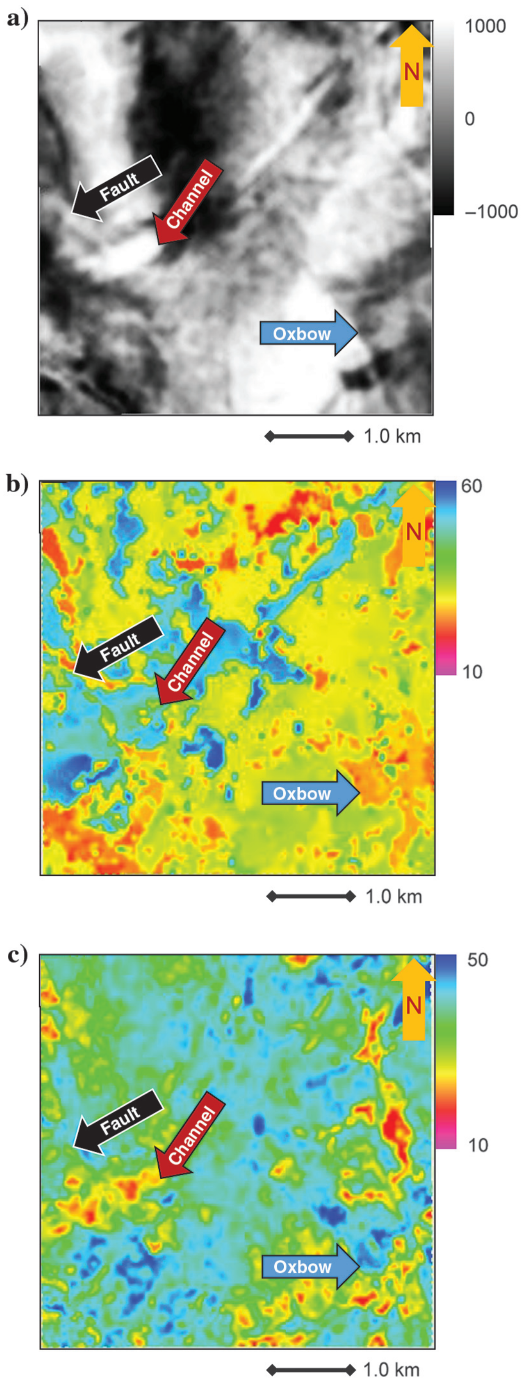

Figure 4. Time slices at $t = 0.5$ s through (a) seismic amplitude, (b) peak frequency, and (c) bandwidth. The dominant frequency is approximately 25 Hz, corresponding to a period of 40 ms.

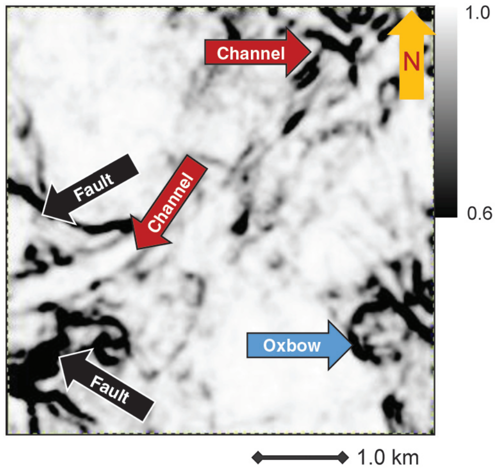

Figure 5. The coherence slice using self-adaptive (0.5–2.0 of the mean period of 20–80 ms) temporal analysis window size of seismic slice in Figure 3.

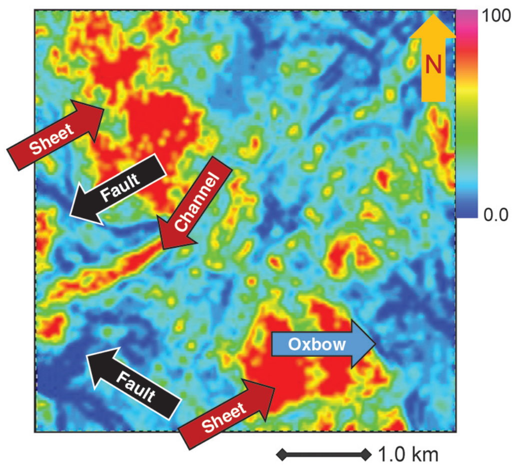

Figure 6. Time slices at $t = 0.5$ s through S/N volumes computed using a self-adaptive temporal analysis window size (0.5–2.0 time of the mean period).

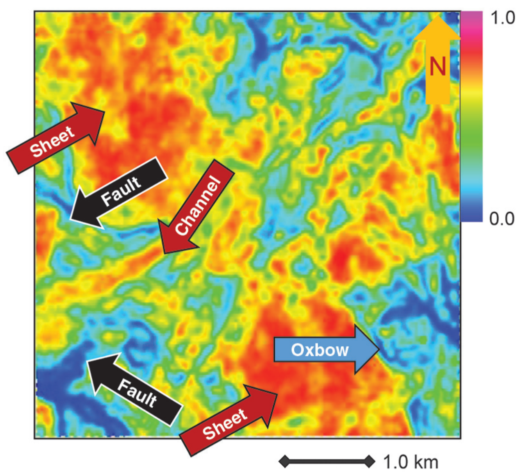

Figure 7. The significance slice using a self-adaptive temporal analysis window size 1.0 times the peak period corresponding to Figure 4b and variable bandwidth from Figure 4c.

coherence image, while maintaining the sharp contrast of faults and channel edges.

Example 3: Structure-oriented filtering based on the statistical significance of coherence

We now apply the significance analysis of coherence to a 3D seismic volume provided by Schlumberger. Figure 8 shows a time slice at $t = 0.7$ s through seismic amplitude; a white arrow indicates a meandering channel, orange arrows indicate three main faults, and red arrows indicate north–south acquisition footprint noise.

Figure 9 shows the coherence slices corresponding to Figure 8 using different color bars, which aid in illustrating the interactive workflow of structure-oriented filtering used to define weights w for the similarity data volumes (Davogustto and Marfurt, 2011) using the color bar to choose appropriate color ramp values of s_{low} and s_{high}. Specifically, we set the color to be white if $s > s_{\mathrm{high}}$, black if $s < s_{\mathrm{low}}$, and shades of gray if $s_{\mathrm{low}} < s < s_{\mathrm{high}}$. The resulting image will be the weights applied to the filtered data on output, such that all black discontinuities will be preserved and all white areas will be filtered.

By modifying the threshold values for s, we increase or decrease the smoothing weights thereby changing the aggressiveness of the filter. In Figure 9a ($s_{\mathrm{high}} = 0.9$, $s_{\mathrm{low}} = 0.7$), we adjust the color bar to enhance the footprint noise (red arrows), as well as structural and stratigraphic features (white and orange arrows). Figure 9b ($s_{\mathrm{high}} = 0.99$, $s_{\mathrm{low}} = 0.97$) indicates the preservation of structures indicated by green arrows, greater improvement of features indicated by blue arrows, and clearer suppression of the footprint noise in the significance of coherence slice. Furthermore, according to the definition of the significance of the coherence, it shows us the statistical conclusion, which holds physical meaning. By estimating the significance of coherence, we can easily suppress the footprint noise, as well as other random noise, because they can be separated from structural anomalies compared with the ones in coherence. Consequently, more null hypotheses (no anomaly) are rejected in structure-oriented filtering by using significance than by using statistical significance of coherence, which can be found in Figure 10.

Figure 10a and 10b shows the result of filtering the data in Figure 8 using structure-oriented filtering based on similarity and statistical significance of coherence. The red arrows in Figure 8 indicate footprint, the amplitude of the footprint in Figure 10 is diminished, whereas the sturctural features are sharpened. Although there are still remnants of footprint noise visible in Figure 10a, it is almost removed in Figure 10b using the significance low threshold. Yellow arrows indicate residual footprint noise that cannot be removed; this is because the values of the coherence and significance of the artifacts are similar to those of the stratigraphic features. We have to keep the artifacts features to preserve the real features of coherence.

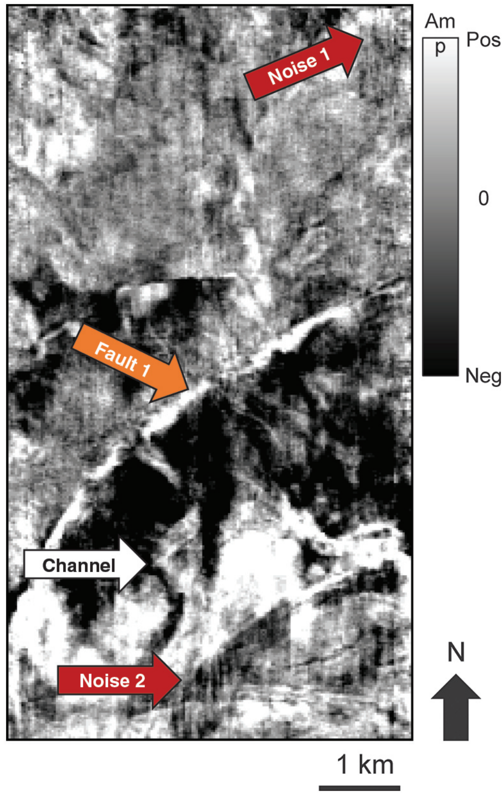

Figure 8. Time slice at $t = 0.75$ s through seismic amplitude.

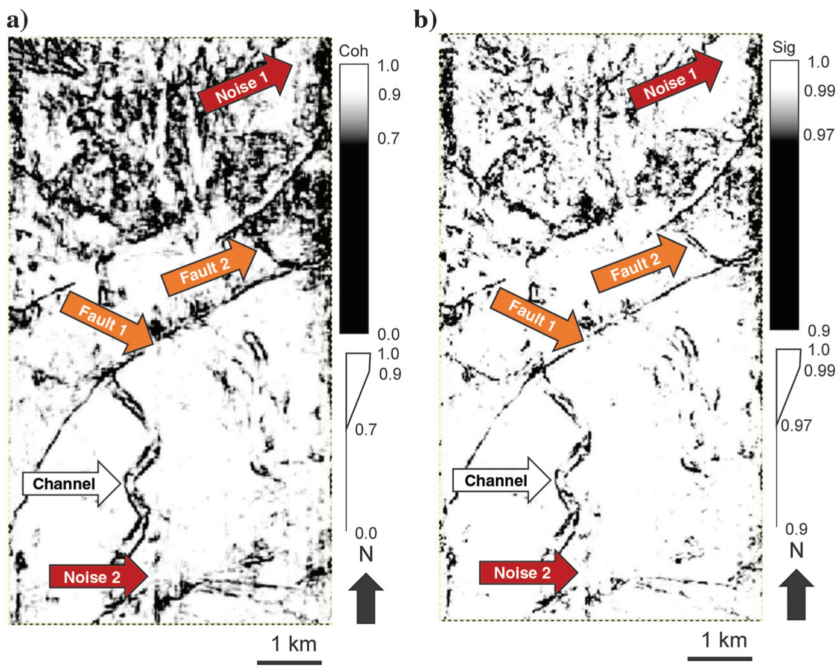

Figure 9. Time slice at $t = 0.75$ s through (a) coherence using a self-adaptive temporal analysis window size and (b) significance of coherence of Figure 7.

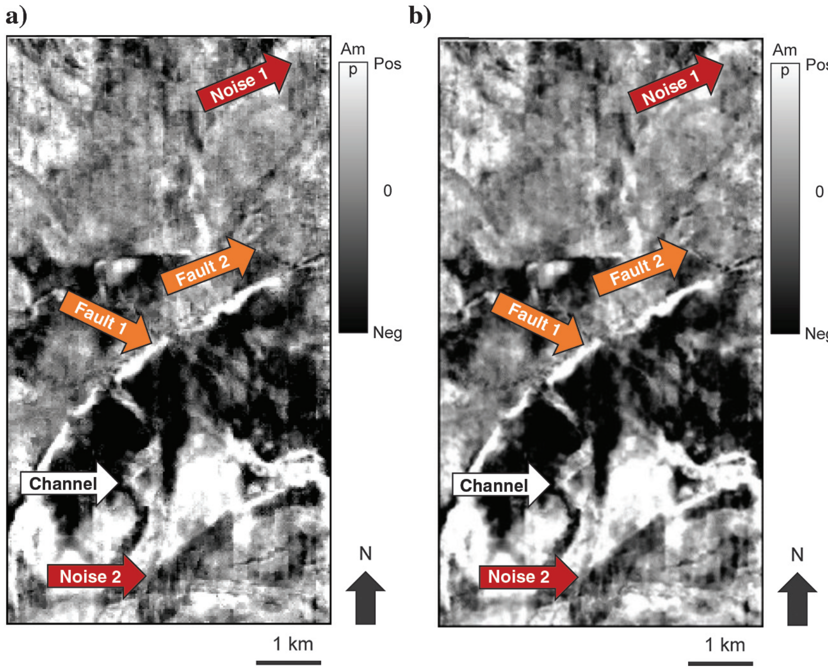

Figure 10. Time slices at $t = 0.75$ s through the output (filtered) seismic amplitude using structure-oriented filtering based on (a) similarity and (b) statistical significance of coherence.

Conclusions

We have generalized analysis on the significance of velocity spectra to grantify the significance of coher-ence anomalies used in 3D interpretation and to con-trol structure-oriented filtering. Four factors control the significance calculation: vertical window size, bandwidth, the number of seismic traces number, and the S/N. The vertical window size is the most im-portant of these four factors and plays an important role in both the degrees of the freedom and the non-centrality parameter ε. We estimate the S/N using a dis-similarity calculation. This estimate is the data adaptive windows that improve the significance. Be-sides, the estimation of significance is subjected to the calculation cost; while equally important, the use of significance helps to determine parameters for edge-preserving structure-oriented filtering. The footprint noise as well as other random noise can be distin-guished from structural anomalies contrast to the one as shown in coherence. Therefore, more null hypoth-esis (no anomaly) can be rejected in structure-oriented filtering using statistical significance of coherence than the one using statistical significance of coher-ence. In the future, we will keep our study in realizing the variable-horizontal window size.

Acknowledgement

We thank the industry sponsors of the University of Oklahoma Attribute-Assisted Seismic Processing and Interpretation for their technical guidance and financial support. Thanks CGG Veritas for providing the survey for use in this survey. Special thanks to Tesseral Technologies for their Tesseral software used in modeling.

Appendix A

Mathematical background

The covariance matrix, semblance, and KL-filter estimates of coherence

Taner and Koehler (1969) define the semblance s of a collection of J seismic traces u_j within a $2K+1$ sample vertical analysis window to be the ratio of the energy of the average trace to the average energy of the individual traces (as shown in Figure 1). The traditional estimate of semblance is thus

$$s(z)=\frac{\sum_{k=-K}^{+K}\alpha_k\left\{\left[\sum_{j=1}^{J}\beta_j u_j(z+k\Delta z)\right]^2+\left[\sum_{j=1}^{J}\beta_j u_j^H(z+k\Delta z)\right]^2\right\}}{\sum_{k=-K}^{+K}\alpha_k\left\{\sum_{j=1}^{J}\beta_j[u_j^2(z+k\Delta z)+u_j^{H^2}(z+k\Delta z)]\right\}}, \tag{A-1}$$

where $u_j(z)$ denotes the measured amplitude of the jth trace at sample z, α_k is the weights applied to the kth sample, and β_j is the weights applied to the jth trace. Traditionally, $\beta_j = 1/J$, where the J traces fall within a user-defined elliptical or rectangular analysis window. T. Lin (personal communication, 2015) shows how one can generalize equation A-1 for radially tapered analysis windows, where the radius and tapering of the analysis window are defined by some measure of the time or time- and space-varying spectrum. Generalization of equations requires one to first compute the covariance matrix $\mathbf{C}$

$$C_{jl}=\sum_{k=-K}^{+K}\alpha_k\left\{\sum_{j=1}^{J}\beta_j[u_j(z_j+k\Delta z)u_l(z_j+k\Delta z)\right.$$
$$\left.+u_j^H(z_j+k\Delta z)u_l^H(z_j+k\Delta z)]\right\}. \tag{A-2}$$

Along dipping horizon z_j, where we have augmented the data sample vectors u_j by its Hilbert transform, u_j^H to provide more robust estimates for small windows about zero crossings. We will use the same tapering windows described by T. Lin (personal communication, 2015), although the subsequent description is appropriate for any tapering function. Specifically, we define

$$\alpha_k = \begin{cases} \frac{1}{2}\left[1+\cos\left(\frac{\pi k \Delta z}{Z}\right)\right] & k\Delta z < Z \\ 0 & k\Delta z \geq Z \end{cases}, \tag{A-3}$$

here

$$Z = (K+1)\Delta z = \frac{\gamma}{\kappa_{\mathrm{ref}}} + \Delta z, \tag{A-4}$$

where κ_{ref} is the reference wavenumber (a percentile p of the local wavenumber spectrum) and γ represents a fraction of this reference window (e.g., 1.0 times the reference window). The final term Δz increases the computational window, such that samples $\pm K$ will always have a nonzero value.

The radial analysis window will have weights

$$\beta_j = \begin{cases} \frac{1}{2}\left[1+\cos\left(\frac{\pi r_j}{R}\right)\right] & r_j < R \\ 0 & r_j \geq R \end{cases}, \tag{A-5}$$

where

$$r_j = (x_j^2 + y_j^2)^{1/2} \tag{A-6}$$

and

$$R = \frac{\gamma}{\kappa_{\mathrm{ref}}} + \mathrm{MIN}(\Delta x, \Delta y). \tag{A-7}$$

Using these weights, T. Lin (personal communication, 2015) computes the semblance of a radially tapered analysis window to be

$$c_s(z) = \frac{\mathbf{aTCa}}{\mathrm{Tr}(\mathbf{C})}, \tag{A-8}$$

where the mathematical trace $\mathrm{Tr}(\mathbf{C})$ of the covariance matrix $\mathbf{C}$ is defined as

$$\mathrm{Tr}(\mathbf{C}) = \sum_{j=1}^{J} C_{jj} \tag{A-9}$$

and where

$$a_j = \left(\frac{\beta_j}{\sum_{l=1}^{J}\beta_l}\right)^{1/2}. \tag{A-10}$$

We will wish to apply our F-statistic estimate of the significance to not only semblance but also to KL-filtered (energy ratio) coherence anomalies. This later estimate is (T. Lin, personal communication, 2015)

$$c_{\mathrm{KL}}(z) = \frac{\sum_{k=-K}^{+K}\alpha_k\left\{\sum_{j=1}^{J}\beta_j[U_j^2(z_j+k\Delta z)+U_j^{H2}(z_j+k\Delta z)]\right\}}{\sum_{k=-K}^{+K}\alpha_k\left\{\sum_{j=1}^{J}\beta_j[u_j(z_j+k\Delta z)+u_j^{H}(z_j+k\Delta z)]^2\right\}}, \tag{A-11}$$

where $U_l(z_l)$ and $U_l^H(z_l)$ are the Karhunen-Loeve-filtered versions of the original data.

Because they consider coherent energy to be signal and incoherent energy to be noise on common midpoint seismic gathers, Douze and Laster (1979) are able to estimate the S/N from the numerator and denominator of the semblance computation

$$s = \frac{\sum_{k=-K}^{+K}\left[\frac{1}{J}\sum_{j=1}^{J}u_j(t+k\Delta t)\right]^2}{\sum_{k=-K}^{+K}\frac{1}{J}\sum_{j=1}^{J}[u_j^2(t+k\Delta t)]} = \frac{P_{\mathrm{S}}}{P_{\mathrm{S}}+P_{\mathrm{N}}}. \tag{A-12}$$

In this case, the S/N $P_{\mathrm{S}}/P_{\mathrm{N}}$ is simply

$$\left(\frac{P_{\mathrm{S}}}{P_{\mathrm{N}}}\right)_s = \frac{\sum_{k=-K}^{+K}\left[\frac{1}{J}\sum_{j=1}^{J}u_j(t+k\Delta t)\right]^2}{\sum_{k=-K}^{+K}\frac{1}{J}\left\{\left[\sum_{j=1}^{J}u_j(t+k\Delta t)\right]^2-\sum_{j=1}^{J}[u_j^2(t+k\Delta t)]\right\}}, \tag{A-13}$$

which varies between zero and infinity.

For our attributes calculation, the S/N for equation A-11 is

$$\left(\frac{P_{\mathrm{S}}}{P_{\mathrm{N}}}\right)_{\mathrm{KL}} = \frac{\sum_{k=-K}^{+K}\alpha_k\left\{\sum_{j=1}^{J}\beta_j[U_j^2(z_j+k\Delta z)+U_j^{H2}(z_j+k\Delta z)]\right\}}{\sum_{k=-K}^{+K}\alpha_k\left\{\sum_{j=1}^{J}\beta_j[u_j^2(z_j+k\Delta z)+u_j^{H2}(z_j+k\Delta z)]^2-\sum_{j=1}^{J}\beta_j[U_j^2(z_j+k\Delta z)+U_j^{H2}(z_j+k\Delta z)]\right\}}. \tag{A-14}$$

For seismic interpreters, high coherence indicates a high S/N. However, low semblance or coherence has four interpretations:

1) a sharp discontinuity, which may indicate the presence of a fault, channel edge, or erosional surface (i.e., the presence of planar geologic features)
2) a relatively diffuse low-coherence pattern, which may indicate the presence of karst collapse, hydrothermally altered dolomite, and mass transport complexes (i.e., the presence of chaotic geologic features)
3) a relatively diffuse low-coherence pattern that is associated with low reflectivity or inaccurate velocities, and hence inaccurate imaging, which may indicate the presence of salt diapirs, overpressured shales, and gas chimneys (i.e., an indicator rather than an image of the geology at a given voxel)
4) a relatively diffusive low-coherence pattern associated with random noise, operator aliasing, acquisition footprint, or overprinted multiples (i.e., the absence of geologic signal, and hence the presence of seismic noise).

Although we will not be able to differentiate cases 3 and 4 described above, our more limited goal is to differentiate diffuse low-coherence anomalies from high-coherence reflectors and planar low-coherence anomalies. One way to estimate such an S/N is to use the disorder attribute.

Disorder

Al-Dossary et al. (2014) introduce a "disorder" attribute that passes not only coherent reflectors but also vertically and horizontally oriented low-coherence anomalies as signal, and thus separates these two geologic patterns from diffuse low-coherence patterns. His original algorithm cascades second derivatives in the x-, y-, and z-directions on a window of the energy (or the power) of the data. This is equivalent to squaring the data, and then filtering it with a $3 \times 3 \times 3$ operator

$$\mathbf{L} = \left\{ \begin{bmatrix} 1 & -2 & 1 \\ -2 & 4 & -2 \\ 1 & -2 & 1 \end{bmatrix}, \begin{bmatrix} -2 & 4 & -2 \\ 4 & -8 & 4 \\ -2 & 4 & -2 \end{bmatrix}, \begin{bmatrix} 1 & -2 & 1 \\ -2 & 4 & -2 \\ 1 & -2 & 1 \end{bmatrix} \right\}. \tag{A-15}$$

The original algorithm suffers from two main drawbacks: (1) it is sensitive to the local average amplitude and (2) it gives rise to diagonal artifacts. To compensate for the local average amplitude sensitivity, Ha (2014) slightly modifies the algorithm to compute disorder D by normalizing the attribute by the root-mean-square magnitude of the windowed data

$$D = \frac{\mathbf{L} \cdot \mathbf{e}}{\|\mathbf{L}\| \|\mathbf{e}\| + \varepsilon}, \tag{A-16}$$

where $\mathbf{L}$ is given by equation A-15, $\mathbf{e}$ is a volume of amplitude energy, the dot indicates a triple inner product, $\|\mathbf{L}\|$ and $\|\mathbf{e}\|$ indicate the L_2-norm, or magnitude, of the operator and data, and ε is a small number to prevent division by zero. To minimize diagonal artifacts, we compute the standard deviation of this attribute along structural dip.

Estimation of fault-plane dip and azimuth using eigenvector analysis

Randen et al. (2000) show how one can estimate the dip and azimuth of a fault (or other planar) discontinuity through the use of the eigenvectors of a coherence-weighted distance matrix $\mathbf{G}$ defined over a window of $M = J * (2K + 1)$ data points within an analysis window by

$$G_{ij} = \frac{\sum_{m=1}^{M} x_{im} x_{jm} \gamma_m}{\sum_{m=1}^{M} \gamma_m}, \tag{A-17}$$

where $\gamma_m = 1 - c_m$ is the similarity, c_m is the coherence at the mth data point, and x_{im} is the distance from the center of the analysis window along axis i of the mth data point. Because we are interested in estimating anomalous behavior, we use γ_m, where most values are close to 0.0, rather than coherence c_m, which has values close to 1.0. The matrix $\mathbf{G}$ has three eigenvalues λ_j and eigenvectors $\mathbf{v_j}$. By construction

$$\lambda_1 \geq \lambda_2 \geq \lambda_3. \tag{A-18}$$

The first eigenvalue λ_1 represents the amount of variance defined by the first eigenvector $\mathbf{v_1}$. Similarly, the second eigenvalue λ_2 represents the amount of variance defined by the second eigenvector $\mathbf{v_2}$. These first two eigenvalues and eigenvectors represent the amount of variance defined by $\mathbf{v_1}$ and $\mathbf{v_2}$. Following Kirlin and Done (1999), a truly chaotic pattern will have

$$\lambda_1 = \lambda_2 = \lambda_3. \tag{A-19}$$

The third eigenvalue λ_3 can thus serve as an estimate of S/N if it is normalized. To be large, there are two conditions to be taken into consideration. First, there need to be some nonzero values of γ_m if any of the eigenvalues are to be nonzero. Second, the distribution of these finite values needs to be random rather than linear or planar, thereby representing either seismic or geologic noise as described by scenarios 3 and 4 above.

Statistical significance of coherence estimates

With this background, we can now estimate the significance of a given semblance or energy ratio coherence estimate. Following Douze and Laster (1979), we approximate the F-statistic with d_1 and d_2 degrees of freedom and noncentrally parameter ε (Blandford, 1974) as

$$F_s(d_1, d_2, \varepsilon) = \frac{(J-1)\sum_{k=-K}^{+K} \alpha_k \left\{ \left[\sum_{j=1}^{J} \beta_j u_j(t+k\Delta t) \right]^2 + \left[\sum_{j=1}^{J} \beta_j u_j^H(t+k\Delta t) \right]^2 \right\}}{\sum_{k=-K}^{+K} \alpha_k \left\{ \sum_{j=1}^{J} \beta_j [u_j^2(t+k\Delta t) + u_j^{H2}(t+k\Delta t)] - \left[\sum_{j=1}^{J} \beta_j u_j(t+k\Delta t) \right]^2 + \left[\sum_{j=1}^{J} \beta_j u_j^H(t+k\Delta t) \right]^2 \right\}} \tag{A-20}$$

and

$$F_c(d_1, d_2, \varepsilon) = \frac{(J-1)\sum_{k=-K}^{+K} \alpha_k \left\{ \sum_{j=1}^{J} [U_j^2(t+k\Delta t) + U_j^{H2}(t+k\Delta t)] \right\}}{\sum_{k=-K}^{+K} \alpha_k \left\{ \sum_{j=1}^{J} \beta_j [u_j^2(t+k\Delta t) + u_j^{H2}(t+k\Delta t)] - \sum_{j=1}^{J} [U_j^2(t+k\Delta t) + U_j^{H2}(t+k\Delta t)] \right\}}, \tag{A-21}$$

where

$$d_1 = f_B \sum_{k=-K}^{+K} \alpha_k \Delta t, \tag{A-22a}$$

$$d_2 = d_1 \sum_{j=1}^{J} \beta_j, \tag{A-22b}$$

and

$$\varepsilon = J d_1 \left(\frac{\mathrm{S}}{\mathrm{N}} \right)^2, \tag{A-22c}$$

where f_B is the bandwidth of the signal in Hz, and S/N is the signal-to-noise ratio we obtain from equations A-13 and A-14.

References

Al-Dossary, S., Y. E. Wang, and M. McFarlane, 2014, Estimating randomness using seismic disorder: Interpretation, **2**, no. 1, SA93–SA97, doi: 10.1190/INT-2013-0088.1.

Blandford, R. R., 1974, An automatic event detector at the Tonto Forest seismic observatory: Geophysics, **39**, 633–643, doi: 10.1190/1.1440453.

Davogustto, O., and K. J. Marfurt, 2011, Removing acquisition footprint from legacy data volumes: 81st Annual International Meeting, SEG, Expanded Abstracts, 1025–1028.

Douze, E. J., and S. J. Laster, 1979, Statistics of semblance: Geophysics, **44**, 1999–2003, doi: 10.1190/1.1440953.

Ha, T., 2014, Seismic attribute illumination of tectonic deformation in Chicontepec basin, Mexico: Master's thesis, University of Oklahoma.

Hoecker, C., and G. Fehmers, 2002, Fast structural interpretation with structure-oriented filtering: The Leading Edge, **21**, 238–243, doi: 10.1190/1.1463775.

Kirlin, R. L., and W. J. Done, 1999, Covariance analysis for seismic signal processing: SEG.

Lin, T., D. Chang, B. Zhang, J. Guo, and K. J. Marfurt, 2014, Seismic attributes estimation using a self-adaptive window: 84th Annual International Meeting, SEG, Expanded Abstracts, 1654–1658.

Marfurt, K. J., 2006, Robust estimates of reflector dip and azimuth: Geophysics, **71**, no. 4, P29–P40, doi: 10.1190/1.2213049.

Marfurt, K. J., R. L. Kirlin, S. L. Farmer, and M. S. Bahorich, 1998, 3-D seismic attributes using a semblance-based coherency algorithm: Geophysics, **63**, 1150–1165, doi: 10.1190/1.1444415.

Neidell, N. S., and M. T. Taner, 1971, Semblance and other coherency measurements for multichannel data: Geophysics, **36**, 482–497, doi: 10.1190/1.1440186.

Randen, T., E. Monsen, C. Signer, A. Abrahamsen, J. O. Hansen, T. Sceter, J. Schlaf, and L. Sonneland, 2000, Three-dimensional texture attributes for seismic data analysis: 70th Annual International Meeting, SEG, Expanded Abstracts, 668–671.

Taner, M. T., and F. Koehler, 1969, Velocity spectra — Digital computer derivation and application of velocity functions: Geophysics, **34**, 859–881, doi: 10.1190/1.1440058.

Tengfei Lin received a B.S. (2011) in seismic exploration from the China University of Petroleum (Huadong), and an M.S. (2014) in geophysics from the University of Oklahoma (OU). He currently is a Ph.D. candidate of geophysics at OU. In the summer of 2011 and 2012, he did two internships at the China National Petroleum Company in Zhuozhou Hebei and Beijing of China. His research interests include seismic processing, velocity analysis, attributes analysis of time-depth domain seismic data, and anisotropy analysis.

Kurt J. Marfurt joined the University of Oklahoma (OU) in 2007, where he serves as the Frank and Henrietta Schultz Professor of Geophysics within the ConocoPhillips School of Geology and Geophysics. Recent work has focused on correlating seismic attributes, such as volumetric curvature, impedance inversion, and azimuthal anisotropy with image logs and microseismic measurements with a particular focus on resource plays. In addition to his teaching and research duties at OU, he leads short courses on attributes for SEG and AAPG. His primary research interests include development and calibration of new seismic attributes to aid in seismic processing, seismic interpretation, and reservoir characterization.

Biographies and photographs of the other authors are not available.